Biophysical Journal Volume 103 July 2012 185–194

Mixed Exciton–Charge-Transfer States in Photosystem II: Stark Spectroscopy on Site-Directed Mutants

Elisabet Romero,[†*] Bruce A. Diner,[‡] Peter J. Nixon,[§] Wiliam J. Coleman,[‡] Jan P. Dekker,[†] and Rienk van Grondelle[†]

[†]Department of Physics and Astronomy, Faculty of Sciences, VU University Amsterdam, Amsterdam, The Netherlands; [‡]Central Research and Development Department, Experimental Station, E. I. du Pont de Nemours & Co., Wilmington, Delaware; and [§]Division of Molecular Biosciences, Imperial College London, London, United Kingdom

ABSTRACT We investigated the electronic structure of the photosystem II reaction center (PSII RC) in relation to the light-induced charge separation process using Stark spectroscopy on a series of site-directed PSII RC mutants from the cyanobacterium *Synechocystis* sp. PCC 6803. The site-directed mutations modify the protein environment of the cofactors involved in charge separation (P_{D1}, P_{D2}, Chl_{D1}, and Phe_{D1}). The results demonstrate that at least two different exciton states are mixed with charge-transfer (CT) states, yielding exciton states with CT character: $(P_{D2}^{\delta+}P_{D1}^{\delta-}Chl_{D1})^*_{673nm}$ and $(Chl_{D1}^{\delta+}Phe_{D1}^{\delta-})^*_{681nm}$ (where the subscript indicates the wavelength of the electronic transition). Moreover, the CT state $P_{D2}^{+}P_{D1}^{-}$ acquires excited-state character due to its mixing with an exciton state, producing $(P_{D2}^{+}P_{D1}^{-})^{\delta*}_{684nm}$. We conclude that the states that initiate charge separation are mixed exciton-CT states, and that the degree of mixing between exciton and CT states determines the efficiency of charge separation. In addition, the results reveal that the pigment-protein interactions fine-tune the energy of the exciton and CT states, and hence the mixing between these states. This mixing ultimately controls the selection and efficiency of a specific charge separation pathway, and highlights the capacity of the protein environment to control the functionality of the PSII RC complex.

INTRODUCTION

The primary photochemical event in photosynthesis is light-induced charge separation. This process takes place in the membrane-bound, photochemically active reaction center (RC), a pigment-protein complex found in nonoxygenic photosynthetic bacteria and oxygen-evolving organisms (cyanobacteria, algae, and higher plants). The charge-separated state created in the RC of photosystem II (PSII) drives water splitting and generates an electrochemical gradient across the membrane that is used to generate ATP and reduce $NADP^+$. Understanding the molecular mechanisms that lead to charge separation is crucial because the success of photosynthesis depends on the efficiency of this process.

Primary charge separation in PSII can be studied in isolated PSII RC complexes that comprise the D_1-D_2-Cyt b_{559} subunits, as well as in larger core complexes. Structural studies on PSII core complexes (1–5) have confirmed that four chlorophyll (Chl), two pheophytin (Phe), and two quinone (Q) molecules bound to the D_1-D_2 heterodimeric RC complex are arranged in two symmetric branches (D_1 and D_2) across the membrane in the center of the complex (Fig. 1). Two additional Chl molecules, $Chls_Z$, are located at opposing sites on the periphery of the D_1-D_2 complex, with two β-carotene molecules situated between the peripheral $Chls_Z$ and the center of the complex. The spatial distribution of the central cofactors (Phe_{D1}, Chl_{D1}, P_{D1}, P_{D2}, Chl_{D2}, and Phe_{D2} (where the subscript indicates the protein branch where the cofactors are localized)) gives rise to a system of coupled pigments that interact, creating collective excited (exciton) states with contributions from various cofactors. In addition, the system is not static. Fast nuclear motions (intra- and interpigment vibrations and protein vibrations) and slow conformational motions of the protein produce homogeneous and inhomogeneous broadening, respectively, of the electronic transitions. Therefore, after a photon is absorbed by the RC, the excitation energy is distributed among the cofactors (depending on the protein conformation or disorder) and converted into a charge-separated state after a series of energy and electron transfer reactions. This means that charge separation can be initiated from different combinations of cofactors (6,7) giving rise to different charge separation pathways (8–13).

Theoretical (11,13) and experimental (12) studies have demonstrated the presence of at least two different low-energy exciton states—$(Chl_{D1}Phe_{D1})^*$ and $(P_{D1}P_{D2}Chl_{D1})^*$—in the PSII RC of higher plants, leading to two different charge separation pathways (note that the cofactors sequence corresponds with their order of participation in the excitonic wavefunction). The choice of a certain charge separation pathway by a single RC complex in the ensemble is strongly dependent on disorder (protein conformation). The sequences of states for the two charge separation pathways, the so-called Chl_{D1} and P_{D1} paths, are as follows:

$$Chl_{D1}\ \text{path}: (Chl_{D1}Phe_{D1})^* \rightarrow Chl_{D1}^{+}Phe_{D1}^{-} \rightarrow P_{D1}^{+}Phe_{D1}^{-}$$

$$P_{D1}\ \text{path}: (P_{D1}P_{D2}Chl_{D1})^* \rightarrow P_{D2}^{+}P_{D1}^{-} \rightarrow P_{D1}^{+}Chl_{D1}^{-} \rightarrow P_{D1}^{+}Phe_{D1}^{-}.$$

Submitted April 2, 2012, and accepted for publication June 12, 2012.

*Correspondence: eli@few.vu.nl

William J. Coleman's present address is Industrial Products Division, Intrexon, San Carlos, CA

Editor: Laura Finzi.

0006-3495/12/07/0185/10 $2.00

http://dx.doi.org/10.1016/j.bpj.2012.06.026

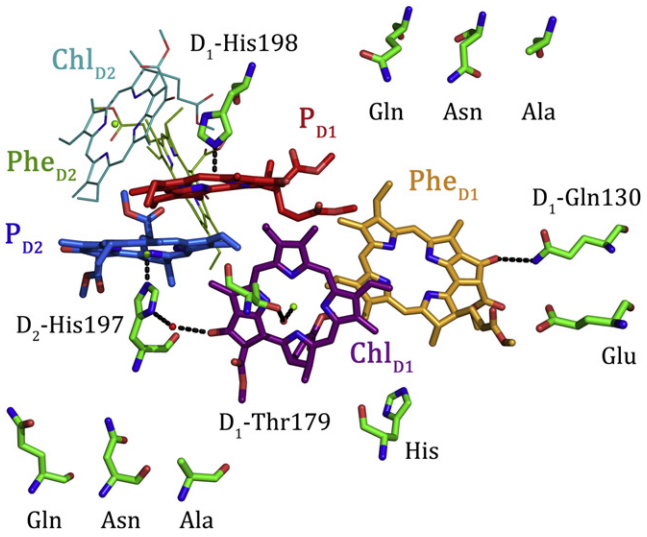

FIGURE 1 Relative positions of the central cofactors in the PSII RC complex together with the positions of the mutated residues (D_1-Gln130, D_1-His198, D_2-His197, and D_1-Thr179) and the chemical structures of the introduced residues (Glu, Gln, Asn, Ala, and His; adapted from Umena et al. (5), Protein Data Bank ID: 3ARC). Water molecules are depicted in red; for the cofactors, the magnesium atoms are in green; for the residues, carbon atoms are in green, oxygen is in red, and nitrogen is in blue.

The participation of an exciton in the primary charge separation reaction (exciton* → radical pair (RP)) depends on its degree of mixing with a charge transfer (CT) state. As a consequence of the mixing, the CT state becomes dipole-allowed because it borrows some dipole strength from the exciton state. In the same way, the static dipole moment of the exciton state increases considerably, which manifests as a significant dipole moment increase in the excited state with respect to the ground state. An extremely sensitive technique for measuring dipole moment changes ($\Delta\mu$) is Stark spectroscopy (11,14,15), which monitors the changes in absorption or emission spectra in the presence of an externally applied electric field. Three molecular parameters can be obtained from the Stark spectra: the change in dipole strength, the change in dipole moment ($\Delta\mu$), and the change in polarizability ($\Delta\alpha$) between the ground and excited state for an electronic transition. $\Delta\mu$ is a measure of the degree of charge redistribution in the excited state associated with a transition. $\Delta\alpha$ is a measure of the deformability of the electronic structure of the states involved in the transition (14,15). By examining the Stark effect on the absorption spectrum, one can monitor the electronic changes that occur directly upon photoexcitation, and thus study the electronic structure of the excited states. The externally applied electric field enhances differentiation between the states that experience a large modification of the electronic density distribution in the excited state (with respect to the ground state), and the states that maintain the ground state electronic structure in the excited state.

The Stark spectrum ($Abs_{Field\ on}$ minus $Abs_{Field\ off}$) for isolated absorption bands in a nonoriented, immobilized sample is described by the Liptay formalism as a linear combination of the zeroth, first, and second derivatives of the absorption spectrum (16). The molecular parameters $\Delta\alpha$ and $\Delta\mu$ scale with the first and second derivatives, respectively, of the absorption spectrum (the classic Stark effect). The shape of the Stark spectrum of PSII RC from higher plants was shown in a previous study (17) to be dominated by the second derivative of the absorption spectrum (2DerAbs) and therefore by $\Delta\mu$. However, in that work deviations from the classic Stark effect were found at wavelengths > 675 nm where the Stark spectrum was red shifted with respect to the 2DerAbs (the nonclassic Stark effect, which is not included in the Liptay formalism). This highlights the limitations of the Liptay formalism when applied to the PSII RC: it cannot describe either the presence of excitonic interactions or the mixing of excitons and CT states (nonclassic Stark effects). To investigate these nonclassic effects and their consequences on the Stark line shape and amplitude, a more sophisticated theoretical model is needed. To that end, Novoderezhkin et al. (11) developed an exciton model based on a quantitative simultaneous fit of the absorption, linear dichroism, circular dichroism, steady-state fluorescence, triplet-minus-singlet, and Stark spectra together with the spectra of pheophytin-modified RCs, and so-called RC5 complexes that lack one of the peripheral Chls. The line-shape functions were expressed in terms of the modified Redfield approach. In this model, the excited-state manifold consists of the excited states of the eight chlorine cofactors (Phe_{D1}, Chl_{D1}, P_{D1}, P_{D2}, Chl_{D2}, Phe_{D2}, Chl_{ZD1}, and Chl_{ZD2}) and one CT state. Of most importance, excitonic interactions, exciton-CT mixing, and coupling to phonons (protein motions) are explicitly included in the model, which allows a consistent modeling of the whole set of experimental data using a unified physical picture. As a result, by including or excluding the excitonic interactions and the mixing of excitons and CT states, the authors were able to investigate the consequences of these nonclassic Stark effects on the line shape and amplitude of the Stark spectrum. To summarize, the fitting of the Stark PSII RC spectrum according to this model shows that 1), excitonic interactions produce band shifts in the Stark spectrum; and 2), exciton-CT mixing produce increased Stark band amplitudes when compared with the 2DerAbs (11). Therefore, comparing the 2DerAbs with the Stark spectrum is a useful tool for qualitatively interpreting the Stark spectrum. Novoderezhkin et al. (11) also showed that the Stark spectrum line shape depends on the energy and configuration of the CT states.

The information contained in the Stark spectra of PSII is difficult to extract due to the spectral congestion in the Q_Y absorption region. To overcome this problem, we chose to use a combined approach: Stark spectroscopy applied to site-directed mutants. In such systems, a specific amino

acid mutation alters the protein environment of a cofactor, i.e., the energy of the exciton and primary RPs states in which the cofactor participates, as well as the exciton-CT mixing. As a result, the line shape and amplitude of the Stark spectra of the mutants changes with respect to the wild-type (WT). These changes can be directly correlated with the energetic changes induced by the mutation as observed in the absorption spectrum, allowing a band assignment that finally leads to a description of the charge separation mechanisms. The mutations studied modify the protein environment of the cofactors involved in charge separation (Phe_{D1}, P_{D1}, P_{D2}, and Chl_{D1}).

Mutants created at residue D_1-130 alter the strength of the hydrogen bond to the 13^1-keto carbonyl of Phe_{D1} (Fig. 1), which leads to significant effects on the quantum yield of primary RP formation (Φ_{RP}) in the isolated PSII RC from *Syn*. In *Syn*. the residue in position D_1-130 is naturally a glutamine (Gln) residue, whereas in higher plants it is a glutamate (Glu). Transient absorption measurements by Giorgi et al. (18) indicated that $\Phi_{RP\ \text{higher plant}} > \Phi_{RP\ \text{D1-Gln130Glu mutant}} > \Phi_{RP\ \textit{Syn.}\ \text{WT}}$. The authors, by considering the $\Phi_{RP\ \text{higher plant}}$ equal to unity, showed that $\Phi_{RP\ \text{D1-Gln130Glu mutant}} \approx 0.75$ and $\Phi_{RP\ \textit{Syn.}\ \text{WT}} \approx 0.55$. The complete removal of the hydrogen-bond interaction in the D_1-Gln130Leu results in an even lower Φ_{RP} ($\approx$0.35). Due to the chemical structure of these residues (Gln contains an amide and Glu contains a carboxylic acid), the strength of the hydrogen bond to the 13^1-keto carbonyl of Phe_{D1} is stronger in higher plants than in cyanobacteria, as shown by Shibuya et al. (19) using FTIR spectroscopy. These authors also showed that the redox potential (E_{red}) of Phe with the 13^1-keto carbonyl hydrogen-bonded with Glu is less negative compared with Gln by 84 mV (19). This means that the strengthening of the hydrogen-bond interaction facilitates the reduction of Phe. In the study presented here, the absorption and Stark spectra of the cyanobacterium *Syn*. PSII RC isolated from the WT and D_1-Gln130Glu mutant strains were compared with those of the PSII RC isolated from a higher plant (spinach).

We investigated the role of the Chls involved in charge separation (P_{D1}, P_{D2}, and Chl_{D1}) in seven site-directed mutants that modify the protein environment of P_{D1} (D_1-His198Gln, D_1-His198Asn, and D_1-His198Ala), P_{D2} (D_2-His197Gln, D_2-His197Asn, and D_2-His197Ala), and Chl_{D1} (D_1-Thr179His; see Fig. 1). All of the introduced mutations allow RC assembly and complete chromophore binding (18,20,21). For the P_{D1} and P_{D2} mutants, the histidine (His) that axially coordinates P_{D1} and P_{D2} is exchanged by glutamine (Gln), asparagine (Asn), or alanine (Ala). The electronic polarizability of the π-system of the imidazole moiety of His stabilizes the excited states of nearby cofactors by dispersive interactions. Therefore, in these mutants, the site energy of P_{D1} or P_{D2} and consequently the exciton states in which P_{D1} and/or P_{D2} participate are expected to shift to the blue (20). In addition, the D_2-His197 mutation is also likely to perturb the energy of the exciton states containing Chl_{D1} because the His residue removed is indirectly hydrogen bonded to the 13^1-keto carbonyl of Chl_{D1} through a water molecule (5). The introduced residues, Gln and Asn, contain an amide moiety that could, directly or indirectly through a water molecule, coordinate the central magnesium of P_{D1} and P_{D2}, or create hydrogen-bond interactions with nearby carbonyls, whereas this is not possible for the alkyl side chain of the Ala residue. For the D_1-Thr179His mutant, the replacement of threonine (Thr), which axially coordinates Chl_{D1} via a water molecule (5), with His is expected to stabilize the Chl_{D1} site energy and consequently the exciton states in which Chl_{D1} participates, producing a red shift in the absorption spectrum of the mutant (21). Previous spectroscopic analyses of these mutants (20,21) led to the assignment of 1), the 683 nm transition to the lowest exciton state in the RC localized mainly on Chl_{D1}; and 2), the 673 nm transition to the low-energy exciton state formed mostly by P_{D1} and P_{D2}.

We report here the comparison of the low-temperature (77 K) absorption and Stark spectra of WT and eight site-directed mutants. The results show that the electronic states that initiate charge separation in PSII RC are mixed exciton-CT states: $(P_{D2}^{\delta+}P_{D1}^{\delta-}Chl_{D1})^*_{673nm}$, $(Chl_{D1}^{\delta+}Phe_{D1}^{\delta-})^*_{681nm}$, and $(P_{D2}^{+}P_{D1}^{-})^{\delta}*_{684nm}$ (where the subscript indicates the wavelength of the electronic transition).

MATERIALS AND METHODS

Sample preparation

PSII RC samples from *Synechocystis* sp. PCC 6803 were prepared as described previously (18). PSII core samples from *Synechocystis* sp. PCC 6803 were prepared as described previously (20,22). The PSII RC isolated from spinach was prepared as described previously (23). The monomeric PSII core samples were analyzed and purified by fast-phase liquid chromatography using a size-exclusion column to eliminate possible PSI contamination and contributions of free Chls and carotenoids to the spectra. The samples were PSI-free, but some contained a significant amount of carotenoid aggregates. The purified samples were diluted in a buffer containing 50 mM MES pH 6.5, 20 mM $CaCl_2$, 5 mM $MgCl_2$, 100 μM $K_3Fe(CN)_6$, 0.03% β-DM, and 57% glycerol (v/v). $K_3Fe(CN)_6$ was added to oxidize Q_A^- to the neutral state and hence keep the RCs open for charge separation. The PSII RC samples were diluted in a buffer containing 20 mM BisTris pH 6.5, 20 mM NaCl, 5 mM $MgCl_2$, 0.09% β-DM, and 57% glycerol (v/v). The addition of $K_3Fe(CN)_6$ is not necessary for the RC samples because Q_A is lost during the isolation procedure.

Spectroscopy

Absorption and Stark spectra were simultaneously recorded at 77 K in a home built setup as described previously (24,25). The optical density of the samples in the Stark cell (thickness 80 μm) was $\approx$0.7 cm^{-1} at 675 nm. The Stark cell was immersed in liquid nitrogen in an Oxford liquid nitrogen cryostat. The Stark cell was rotated 45° with respect to the propagation direction of the horizontally polarized measuring light to set the angle between the electric field component of the light and the externally applied electric field, χ, to the magic angle (54.7°). The Stark spectra

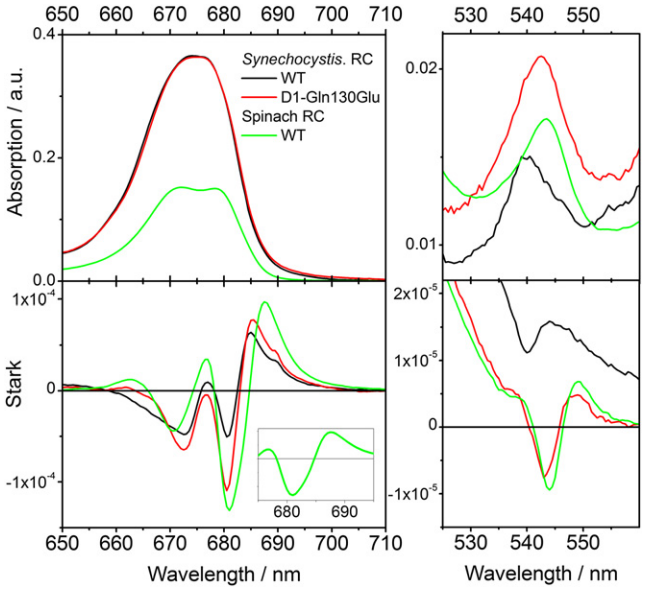

FIGURE 2 Simultaneously recorded 77 K absorption and Stark spectra for the *Synechocystis* PCC 6803 RC complex WT and D_1-Gln130Glu mutant, and the spinach RC complex WT. Left panel: Chl-Phe Q_Y absorption region (*inset*: spinach RC WT 681 nm Stark minimum expanded). Right panel: Phe Q_X absorption region. The absorption and Stark spectra are normalized to the RC content. The Stark spectra were recorded at $\chi = 54.7°$ and at an external electric field strength of 2.25×10^5 V cm^{-1}.

were recorded at an externally applied electric field strength of 2.25×10^5 V cm^{-1}.

RESULTS AND DISCUSSION

Phe_{D1} mutant

The simultaneously recorded 77 K absorption and Stark spectra of the *Syn.* PSII RC WT and D_1-Gln130Glu mutant, and of spinach PSII RC WT (D_1-Glu130) normalized to the RC content are shown in Fig. 2. A comparison of these spectra provides information about the effect of the hydrogen-bond interaction between the residue at position D_1-130 and the 13^1-keto carbonyl of Phe_{D1} on the efficiency of the charge separation process.

Absorption spectra

The amplitude of the *Syn.* RC samples' absorption is higher with respect to the spinach RC because the *Syn.* RC samples are not completely pure. They contain approximately one CP47 antenna complex per two RC complexes, i.e., they are RC-enriched preparations (hereafter called RC complexes). The small differences in the antenna content of the *Syn.* RC complexes hinder the comparison of the WT and mutant absorption line shape. In the Phe Q_X absorption region, the replacement of Gln in WT for Glu in the D_1-Gln130Glu (spinach-like) mutant produces a 2.5 nm red shift of the Phe Q_X band at 540 nm in WT to 542.5 nm in the mutant, as observed previously (18). For the spinach RC, which contains a Glu at position D_1-130, the maximum of the Phe Q_X band peaks at 543.5 nm. The amplitude of the Phe Q_X band is very similar in the three RC preparations, indicating that the normalization procedure is correct.

Stark spectra

The differences in composition between the *Syn.* RC complexes and between *Syn.* and spinach RC have a minor effect on the Stark spectra due to the small contribution to the Stark spectra of the CP47 antenna complex in the absorption regions of interest (with respect to the contribution to the Stark spectra of the RC, see Fig. S1 in the Supporting Material). The Stark spectra of the three RC samples resemble the second derivative of the absorption spectra (2DerAbs; Fig. S2), indicating that, to a first approximation, these Stark spectra are dominated by a change in dipole moment, $\Delta\mu$, between the ground and excited states associated with the electronic transitions. A similar Stark effect was observed in the bacterial RC (26–28) and in the previously reported Stark spectrum of higher plant PSII RC (spinach) (17). In the PSII RC, the Stark spectra are dominated by the excitonically coupled (and coupled to CT states) cofactors located in the active branch (P_{D1}, Chl_{D1}, and Phe_{D1}) and inactive branch (P_{D2}). The monomeric $Chls_Z$, Chl_{D2}, and Phe_{D2} cofactors are not expected to give a significant Stark response (17) because they do not substantially contribute to the collective exciton states (11) that initiate charge separation, i.e., they are not supposed to be mixed with CT states.

The Stark spectrum of the *Syn.* RC WT in the Q_Y absorption region is composed of two negative bands at 672.5 and 680.5 nm, three maxima at 677 and 685 nm, and a shoulder at 689.5 nm. For the D_1-Gln130Glu (spinach-like) mutant, the positions of the Stark bands are virtually identical to those of the WT. The main difference is the twofold increase in amplitude of the negative band at 680.5 nm in the mutant. The Stark spectrum of the spinach RC WT in the Q_Y absorption region is composed of two negative bands at 670.5 and 681 nm, and three maxima at 663, 676.5, and 687.5 nm, as reported previously (17). The Stark band shifts in the spinach RC with respect to the *Syn.* samples may be due to small differences in the energy of the exciton states between the two organisms. The amplitude of the 670.5 nm Stark minimum in the spinach RC is similar to its *Syn.* counterparts, whereas the amplitude of the 681 nm minimum is similar to the 680.5 nm minimum in the D_1-Gln130Glu mutant. It is interesting to note that upon replacement of Gln with Glu in the D_1-Gln130Glu mutant, the amplitude of the 680.5 nm Stark minimum resembles the amplitude of the spinach RC, which also contains a Glu in position D_1-130. In the Phe Q_X absorption region, an amplitude increase of the Phe_{D1} Stark minima is also clearly observed for the D_1-Glu130 samples (*Syn.* mutant and spinach RC WT) with respect to the

D_1-Gln130 sample (*Syn*. RC WT). For the *Syn*. RC WT, the Phe_{D1} Q_X Stark minimum is at 540 nm (i.e., no shift in position between Stark and absorption bands) and its amplitude is 5×10^{-6} (ΔAbs/a.u.), whereas for the D_1-Gln130Glu mutant and the spinach RC WT, the Phe_{D1} Q_X Stark minima are at 542.5 and 543.5 nm (0.5 nm red shift of the Stark spectrum with respect to the absorption band) and their amplitudes are 13×10^{-6} and 15×10^{-6} (ΔAbs/a.u.), respectively.

When interpreting these results, it is important to remember that the replacement of Gln at position D_1-130 by Glu in the D_1-Gln130Glu mutant increases the quantum yield of RP formation (18). Remarkably, the increase of Φ_{RP} correlates with the increase of the Stark minimum amplitude at 680.5–681 nm. In addition, we observe a similar trend when we compare the Stark spectra with the 2DerAbs spectra (Fig. S2): the larger the Stark amplitude with respect to the 2DerAbs spectra, the higher the quantum yield of RP formation. These observations indicate that the Stark spectrum and its comparison with the 2DerAbs spectrum are a direct measure of the quantum yield of RP formation in PSII.

The comparison of the Stark spectra presented in Fig. 2 indicates that 1), Phe_{D1} contributes to the 680.5–681 nm exciton state in the three RC samples analyzed; and 2), the strengthening of the hydrogen-bond interaction between the residue at position D_1-130 and the 13^1-keto carbonyl of Phe_{D1} (in the mutant and spinach RC) enhances the mixing exciton-CT for the 680.5–681 nm state (with respect to *Syn*. WT). According to the experimental evidence presented here (see also "P_{D1}, P_{D2}, and Chl_{D1} mutants" section below) and our model (11–13), the mixing between the exciton $(Chl_{D1}Phe_{D1})^*$ and the CT state $Chl_{D1}^{+}Phe_{D1}^{-}$ generates an exciton with CT character $(Chl_{D1}^{\delta+}Phe_{D1}^{\delta-})^*$ that gives rise to the Stark minimum at 680.5 and 681 nm in the *Syn*. and spinach RC samples, respectively (where δ^+ and δ^- indicate the fraction of CT acquired by the exciton state).

Interestingly, in the red tail of the Stark spectra of the *Syn*. RC samples, a positive shoulder at 689.5 nm is also observed (Fig. 2). The higher amplitude of the shoulder in the *Syn*. RC mutant is most likely due to the overlap with the more intense 680.5 nm Stark band in the mutant with respect to WT, which suggests that the red shoulder is not affected by the mutation. Therefore, the presence of the 689.5 nm shoulder indicates that another state without participation of Phe_{D1} contributes to the intense negative Stark signal at 680.5 nm in the *Syn*. RC samples. In spinach, this shoulder is not resolved in the red positive tail of the Stark spectra (most likely due to spectral overlap with the maximum at 687.5 nm). However, the negative 681 nm Stark band is asymmetric with a shoulder around 684 nm (*inset* in Fig. 2, *bottom-left panel*). This spectral shape suggests that also in spinach more than one state may contribute to the intense negative Stark signal at 681 nm. The presence of two states contributing to the 680.5–681 nm Stark minimum is further supported by the 2DerAbs spectra in which two separated minima are present (Fig. S2). According to our model (11), the CT state $P_{D2}^{+}P_{D1}^{-}$ is strongly mixed with the $(P_{D1}P_{D2})^*$ exciton state. In this case, the CT state borrows dipole strength from the exciton, producing a red-most state $(P_{D2}^{+}P_{D1}^{-})^{\delta*}$ with an absorption centered around 684 nm (where $\delta*$ indicates the fraction of dipole strength acquired by the CT state). Due to its CT character, this state is expected to contribute to the Stark spectra, which will be dominated by $\Delta\mu$ and therefore will resemble the second derivative of the absorption spectra. Thus, we suggest that the $(P_{D2}^{+}P_{D1}^{-})^{\delta*}$ state contributes to the red edge of the 680.5–681 nm Stark minimum. It appears as a positive shoulder at 689.5 nm in the *Syn*. RCs, whereas it appears as a negative shoulder around 684 nm in the spinach RC.

P_{D1}, P_{D2}, and Chl_{D1} mutants

The simultaneously recorded 77 K absorption and Stark spectra of *Syn.* core complex for the WT, D_1-His198Gln, and D_2-His197Gln mutants; WT, D_1-His198Asn, and D_2-His197Asn mutants; WT, D_1-His198Ala, and D_2-His197Ala mutants; and WT and D_1-Thr179His mutant in the Q_Y region are shown in Fig. 3.

The effect of these mutations on the Phe Q_X region is shown and discussed in the Supporting Material (see "The Phe Q_X absorption band" section, Fig. S3, and Table S1).

The PSII core complex analyzed in this section contains the photochemically active RC as well as the core antenna proteins CP43 and CP47. In higher plants (spinach) for which the RC, CP43, and CP47 isolation procedures are well established (23,29–32), the amplitude of the antenna Stark spectra with respect to that of the RC is approximately equal around 670 nm and presents an ≈4-fold decrease around 680 nm (Fig. S1). Taking this finding and the fact that the mutations only affect the cofactors in the RC into account, we will discuss the core complex absorption and Stark spectra in terms of changes within the RC.

Absorption spectra

As a first approximation, we assume that the mutations influence only the energy of the electronic transition of a certain exciton state, and not the transition dipole moment strength or direction. To examine the energy shifts, we normalized the absorption spectra of WT and mutants to the cofactor content and calculated the absorption difference spectra ($Abs_{dif} = Abs_{mutant} - Abs_{WT}$; Fig. 3). In the Abs_{dif} spectra, the negative bands correspond to absorption bands that disappear in the WT upon mutation, and the positive bands correspond to new absorption bands that appear upon mutation.

Three different mutations were constructed at positions D_1-His198 and D_2-His197, which axially coordinate P_{D1} and P_{D2}, respectively. The absorption changes induced

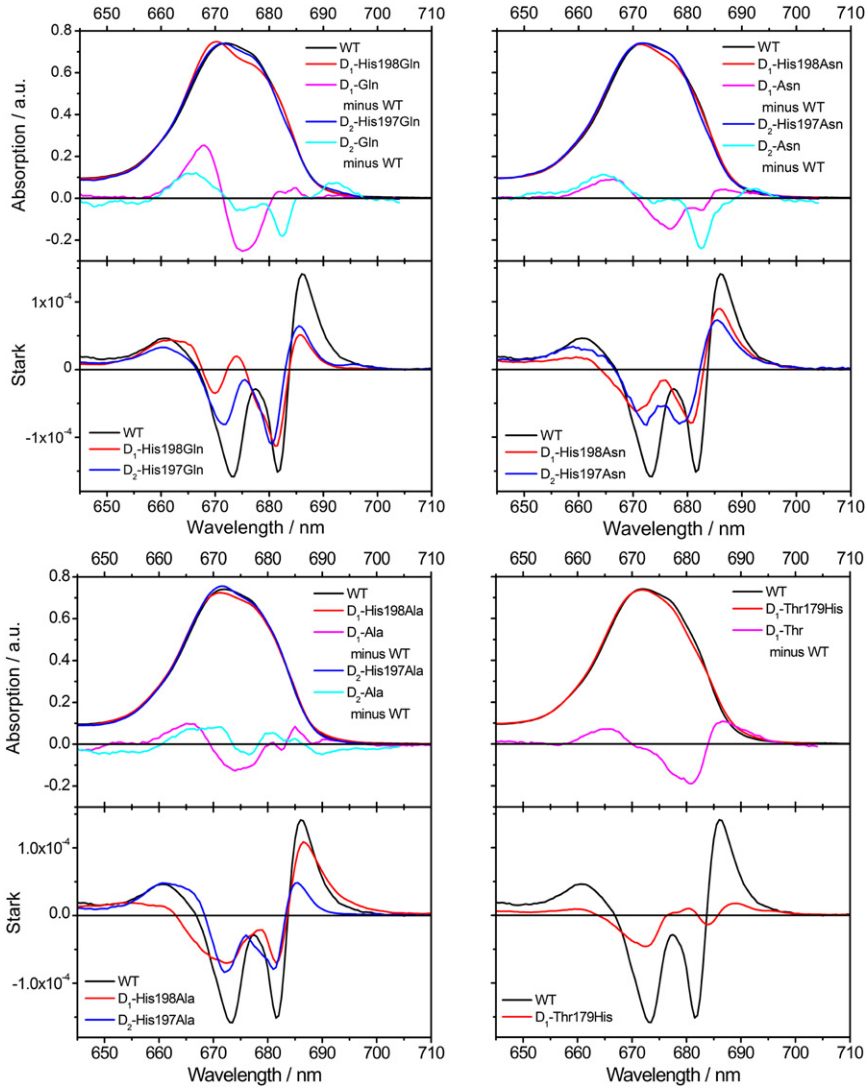

FIGURE 3 Simultaneously recorded 77 K absorption and Stark spectra of the *Synechocystis* PCC 6803 core complex in the Q_Y absorption region for the WT, D_1-His198Gln, and D_2-His197Gln mutants (*top left panel*); WT, D_1-His198Asn, and D_2-His197Asn mutants (*top-right panel*); WT, D_1-His198Ala, and D_2-His197Ala mutants (*bottom-left panel*); and WT and D_1-Thr179His mutant (*bottom right panel*). The absorption and Stark spectra are normalized to the cofactor content. The absorption difference spectra have been multiplied by 5 to facilitate visualization. The Stark spectra were recorded at $\chi = 54.7°$ and an external electric field strength of 2.25×10^5 V cm^{-1}.

by the exchange of His for the amide residues, Gln and Asn, are similar for the D_1 branch mutants, as well as for the D_2 branch mutants (Fig. 3). In the four mutants (D_1-His198Gln, D_1-His198Asn, D_2-His197Gln, and D_2-His197Asn), two minima at around 675 and 683 nm, and one maximum at around 666 nm with different relative amplitude and width are observed in the absorption difference spectra (Fig. 3). For the two D_1-His198 mutants, the main change upon mutation is an apparent blue shift of the 675 nm band to 666 nm, in agreement with the assignment of a band at 673 nm to the low-energy exciton state formed predominantly by P_{D1} and P_{D2} ($P_{D1}P_{D2}$ exciton; see below) (20,21,33), which shifts to the blue upon His replacement. For the D_2-His197 mutants, the amplitude of the 675 nm minimum is significantly smaller, suggesting that P_{D2} participates less than P_{D1} in the $P_{D1}P_{D2}$ exciton. The observed absorption loss at 683 nm is similar for both the D_2-His197 mutants and is assigned to a secondary effect on Chl_{D1}.

This secondary effect on Chl_{D1} has several possible origins: the loss of the hydrogen bond to the 13^1-keto carbonyl makes the Chl_{D1} π-conjugated system less asymmetric and/or the disappearance of the dispersive interactions provided by His (which also stabilizes the exciton states in which Chl_{D1} participates). Both effects are expected to induce a blue shift in the absorption spectrum. Alternatively, the mutation may increase the disorder in the system. In this case, a narrow localized state may become more delocalized to compensate for the higher disorder of the system, i.e., the narrow band broadens. The third explanation is more in line with the second derivative line shape of the Abs_{dif} spectra (Fig. 3). When we compare the effect of the Gln and Asn mutations in the active and inactive branches, it is interesting to note that the main absorption loss has its counterpart, with smaller amplitude, in the other branch mutant, highlighting the presence of excitonic coupling between P_{D1} and P_{D2}.

For both of the D_1 and D_2 Ala mutants, the absorption difference spectra have similar spectral shapes. The minimum at 683 nm is similar in both mutants; the main difference is found in the 675 nm band, which is broader and has higher amplitude in the D_1 mutant. In the Ala mutants, the site-directed mutation (Fig. 1) affects both sides in a similar way, with the D_1 side being the most affected. These observations support the notion that P_{D1} and P_{D2} are energetically coupled, i.e., they contribute to the same exciton state: the low-energy state that is located around 675 nm (with higher participation from P_{D1}) (21,34). The high-energy component of this exciton state is located around 660 nm (34). It has a lower transition dipole moment strength and is therefore not observed in the Abs_{dif} spectra.

The mutation constructed at position D_1-Thr179 (Thr axially coordinates Chl_{D1} via a water molecule (5); Fig. 1) gives rise to a different absorption difference spectral shape with respect to the P_{D1} and P_{D2} mutants. In this case, an asymmetric minimum with contributions from 681, 677, and 671 nm components (in decreasing order of amplitude) and two maxima at 666 and 687 nm are observed. This spectral shape can be understood as a band broadening (the asymmetric minimum broadens to a band extending from 660 to 700 nm with $\approx$25 nm full width at half-maximum (FWHM)) or as a band shift (taking into account the amplitude of the maxima and minima, the 681 nm band red shifts to 687 nm, and the 677 and 671 nm bands blue shift to 666 nm). Recent experimental (21) and theoretical (33) studies on this mutant that showed the red shift of the Chl_{D1} exciton upon Thr exchange by His support the second interpretation. For this mutant, the red shift of the main 681 nm band and the blue shift of the minor 671 and 677 nm bands indicate that Chl_{D1} participates in two excitons: the Chl_{D1} exciton and, to a lesser extent, the $P_{D1}P_{D2}$ exciton. In summary, the results are consistent with the presence of two different low-energy exciton states in the ensemble of PSII RCs (11–13,20,21,35), the $P_{D1}P_{D2}Chl_{D1}$ exciton (the low-energy exciton state that absorbs around 673 nm) and the $Chl_{D1}Phe_{D1}$ exciton state (see "Phe_{D1} mutant" section above, "The Phe Q_X absorption band" section in the Supporting Material, Fig. S3, and Table S1) with absorption around 681 nm, in agreement with the literature. (Note that the order of the cofactors in the exciton nomenclature, $P_{D1}P_{D2}Chl_{D1}$, reflects a decreasing extent of participation in the exciton state.).

Stark spectra

The interpretation of the Stark spectra is based primarily on the comparison of the absorption and Stark spectra between WT and mutants (Fig. 3) in terms of band shifts and differences in band amplitudes, and secondarily on the comparison of the Stark spectra with the second derivative of the absorption spectra (2DerAbs; Fig. S4).

The Stark spectra of the PSII cores, WT, and mutants resemble the second derivative of the absorption spectra (2DerAbs; Fig. S4), indicating that to a first approximation, these Stark spectra are dominated by a change in dipole moment, $\Delta\mu$, between the ground and excited states associated with the electronic transitions. A similar Stark effect was observed in the bacterial RC (26,27) and the higher plant PSII RC (17) (Fig. 2).

The Stark spectrum of the WT is composed of two main minima at 673.25 and 681.75 nm and three maxima located at 661, 677, and 686.25 nm. In the second derivative of the absorption spectrum (Fig. S4), three minima are present at 670, 677.5, and 682.5 nm, and two maxima are present at 661 and 687 nm. The Stark spectrum presents shifts of 1–3 nm (nonclassic Stark effect) and a threefold amplitude increase with respect to the 2DerAbs, which indicates that exciton couplings among the cofactors and exciton-CT mixing, respectively, are present in the WT core complex. For all mutants, band shifts in the Stark spectra with respect to the 2DerAbs are observed, indicating that in the mutants the exciton couplings are also present. However, for all mutants (with the exception of D_2-His197Gln), the amplitudes of the minima of the Stark spectra are of the same order as those of the 2DerAbs spectra, indicating that the mixing with CT states is reduced or absent (Fig. S4). The most significant Stark band positions and amplitudes in the Q_Y region are listed in Table S2.

For all mutants, the blue minimum, at 673.25 nm in the WT, is blue shifted 0.75–3.25 nm and displays a two- to fourfold amplitude decrease upon mutation (Table S2). This blue shift is in agreement with the analysis of the absorption: an exciton band with participation from $P_{D1}P_{D2}Chl_{D1}$ absorbing around 673 nm shifts to the blue upon mutation. According to the order of participation in the exciton state, the shift (for a specific mutation) is more pronounced for the P_{D1} than for the P_{D2} mutants and even less so for the Chl_{D1} mutant.

Thus far, the Stark spectra have confirmed the assignments from the absorption and the literature (20,21). At this point, we will examine the potential of the $P_{D1}P_{D2}Chl_{D1}$ exciton state to initiate charge separation. This potential depends on the degree of mixing between the exciton and CT states: the stronger the mixing, the larger the Stark amplitude and the higher the potential to initiate charge separation (11). The changes in band position and amplitude for the P_{D1} and P_{D2} mutants show a correlation between the blue shift and the amplitude decrease of the 673.25 nm minimum: the stronger the shift, the larger the Stark amplitude reduction (Fig. S5). This correlation indicates that the absorption band shifts induced by the mutations decrease the exciton-CT mixing present in the WT, i.e., in the WT the $(P_{D1}P_{D2}Chl_{D1})^*$ exciton absorbing at 673.25 nm is mixed with the $P_{D2}^{+}P_{D1}^{-}$ CT state (due to the strong overlap between the electronic wavefunctions of these states) (11), yielding the $(P_{D2}^{\delta+}P_{D1}^{\delta-}Chl_{D1})^*$ state. Thus, we conclude that the mixed $(P_{D2}^{\delta+}P_{D1}^{\delta-}Chl_{D1})^*$ state initiates charge separation following the P_{D1} path

$((P_{D2}^{\delta+}P_{D1}^{\delta-}Chl_{D1})^* \rightarrow P_{D2}^{+}P_{D1}^{-} \rightarrow P_{D1}^{+}Chl_{D1}^{-} \rightarrow P_{D1}^{+}Phe_{D1}^{-}$ (12)) in a fraction of the RCs in which this mixed exciton-CT state is the lowest-energy state, and that the relative contribution of this path is strongly reduced in the P_{D1} and P_{D2} mutants.

Concerning the red minimum, at 681.75 nm in the WT, the mutants can be divided into two groups: 1), the P_{D1} and P_{D2} mutants with a blue shift (more significant for the P_{D2} mutations) and decrease in amplitude (similar for P_{D1} and P_{D2} mutants) depending on the specific mutation; and 2), the Chl_{D1} mutant with a red shift and a significant amplitude decrease. Considering the contribution of two exciton-CT states to the red Stark minimum observed in the RC samples, the blue shift present in the P_{D1} and P_{D2} mutants can be understood as a loss of a red component in the red Stark minimum. As discussed above, the P_{D1} and P_{D2} mutations induce a decrease in the $(P_{D1}P_{D2}Chl_{D1})^* \leftrightarrow P_{D2}^{+}P_{D1}^{-}$ mixing that reduces the Stark amplitude of the 673.25 nm Stark minima (the $(P_{D2}^{\delta+}P_{D1}^{\delta-}Chl_{D1})^*$ mixed state has less CT character). In turn, the decrease of the mixing reduces the transition dipole moment of the reddest $P_{D2}^{+}P_{D1}^{-}$ CT state. Therefore, the decrease of the (red) contribution of $P_{D2}^{+}P_{D1}^{-}$ CT state to the Stark spectra appears as a blue shift of the red Stark minimum. The fact that the decrease in Stark amplitude is the same in both P_{D1} and P_{D2} mutants can be explained by considering that the P_{D1} and P_{D2} cofactors contribute equally to the $P_{D2}^{+}P_{D1}^{-}$ CT state. In the case of the 673.25 nm minimum, the mutation effect is more pronounced for the P_{D1} mutants because the contribution of the P_{D1} cofactor to the $(P_{D1}P_{D2}Chl_{D1})^*$ exciton is larger than the contribution of P_{D2}.

In the D_1-Thr179His mutant, the absorption red shift of the exciton with participation of Chl_{D1} produces a substantial amplitude decrease (1/10 of the value for WT) and red shift (3.25 nm with respect to WT) of the red Stark minimum. These observations could be interpreted as a decrease of the Chl_{D1} exciton-CT mixing due to the red shift of the Chl_{D1} exciton absorption. However, the fact that two exciton-CT states contribute to the red Stark minimum and the comparison of the D_1-Thr179His Stark spectra with the 2DerAbs indicate that the situation is more complex. This comparison shows that the 677.75 nm minimum in the 2DerAbs is almost completely absent in the Stark spectrum, and the 684 nm minimum in the 2DerAbs overlaps with the Stark minimum (Fig. S4). These observations indicate that 1), the red shift of the Chl_{D1} exciton absorption in the mutant disrupts the mixing with a CT state present in WT (as suggested by the absence of the 677.75 nm Stark minimum); and 2), the 684 nm minimum corresponds to the Stark contribution of the $(P_{D2}^{+}P_{D1}^{-})^{\delta*}$ state (in agreement with the interpretation of the Stark spectra presented in the "Phe_{D1} mutant" section; Fig. 2). The fact that the 684 nm Stark minimum has the same amplitude as the 2DerAbs (and not a higher one, as would be expected for a state with significant CT character) suggests that the mutation in the environment of Chl_{D1} also affects the electronic properties of the $(P_{D2}^{+}P_{D1}^{-})^{\delta*}$ state.

Taken together, these results lead us to propose that the Stark minimum at 681.75 nm in WT arises from the combination of two different states. On the one hand, the $(Chl_{D1}^{\delta+}Phe_{D1}^{\delta-})^*$ state (produced by the mixing of the $(Chl_{D1}Phe_{D1})^*$ exciton with the $Chl_{D1}^{+}Phe_{D1}^{-}$ CT state) contributes to the blue edge of the 681.75 nm Stark minimum ($\approx$681 nm; see also "The Phe Q_X absorption band" section in the Supporting Material, Fig. S3, and Table S1). On the other hand, the $(P_{D2}^{+}P_{D1}^{-})^{\delta*}$ state (formed by the mixing of the $P_{D2}^{+}P_{D1}^{-}$ CT state with the $(P_{D1}P_{D2}Chl_{D1})^*$ exciton) contributes to the red edge of the 681.75 nm Stark minimum ($\approx$684 nm). Thus, we conclude that the $(Chl_{D1}^{\delta+}Phe_{D1}^{\delta-})^*$ state leads to charge separation via the Chl_{D1} path (12) whenever this exciton is the lowest-energy state of the RC. In addition, direct excitation of the $(P_{D2}^{+}P_{D1}^{-})^{\delta*}$ state leads to charge separation via the P_{D1} path (11).

In summary, we conclude that the electronic states that initiate charge separation are mixed exciton-CT states, not pure exciton states. This finding leads to the following refined charge separation pathways:

P_{D1} path

$$(P_{D2}^{\delta+}P_{D1}^{\delta-}Chl_{D1})^*_{673nm} \rightarrow P_{D2}^{+}P_{D1}^{-} \rightarrow P_{D1}^{+}Chl_{D1}^{-} \rightarrow P_{D1}^{+}Phe_{D1}^{-}$$

Chl_{D1} path

$$(Chl_{D1}^{\delta+}Phe_{D1}^{\delta-})^*_{681nm} \rightarrow Chl_{D1}^{+}Phe_{D1}^{-} \rightarrow P_{D1}^{+}Phe_{D1}^{-}$$

P_{D1} path

$$(P_{D2}^{+}P_{D1}^{-})^{\delta*}_{684nm} \rightarrow P_{D2}^{+}P_{D1}^{-} \rightarrow P_{D1}^{+}Chl_{D1}^{-} \rightarrow P_{D1}^{+}Phe_{D1}^{-},$$

where the subscripts indicate the approximate center wavelength of the electronic transition for each of the mixed states.

This conclusion is in excellent agreement with the results from a high-resolution fluorescence spectroscopy (fluorescence line-narrowing) study by Peterman et al. (36). The authors studied the electronically excited state of PSII RC using fluorescence line-narrowing spectroscopy at 5 K, and compared the obtained spectral features with those obtained earlier for the primary electron donor (37). Their results show that there is a striking resemblance between the emitting and charge-separating states, including a very similar shape of the phonon wing, almost identical frequencies of a number of vibrational modes, a very similar double-Gaussian shape of the inhomogeneous distribution

function, and relatively strong electron-phonon coupling for both states. All of these observations are explained by the fact that the excited states that give rise to charge separation in the PSII RC are mixed exciton-CT states; for instance, strong electron-phonon coupling is expected for states with CT character. It is also interesting to note that the best numerical simulation of the absorption, nonselectively, and selectively excited emission spectra was obtained with an inhomogeneous distribution function consisting of two Gaussians, one peaking at 680.6 nm (width 80 cm^{-1}, relative area 0.91) and the other peaking at 683.6 nm (width 70 cm^{-1}, FWHM) (36). These values are in excellent agreement with the properties and center wavelengths for the $(Chl_{D1}{}^{\delta+}Phe_{D1}{}^{\delta-})^*_{681nm}$ and $(P_{D2}{}^{+}P_{D1}{}^{-})^{\delta*}_{684nm}$ states, respectively, found in our study. The state simulated by a Gaussian band centered at 680.6 nm corresponds to the mixed exciton-CT state $(Chl_{D1}{}^{\delta+}Phe_{D1}{}^{\delta-})^*_{681nm}$, which carries most of the oscillator strength due to its major exciton character. The state simulated by a Gaussian band centered at 683.6 nm corresponds to the mixed CT-exciton $(P_{D2}{}^{+}P_{D1}{}^{-})^{\delta*}_{684nm}$ state with lower oscillator strength due to its minor exciton character (acquired by borrowing oscillator strength from the $(P_{D2}P_{D1}Chl_{D1})^*$ state).

CONCLUSIONS

The results demonstrate that the states that initiate charge separation are mixed exciton-CT or CT-exciton states, not pure exciton states as previously believed. The degree of mixing between exciton and CT states determines the quantum yield of RP formation and therefore the efficiency of charge separation (the higher the mixing, the higher the efficiency of charge separation). The exciton-CT states that initiate charge separation are $(P_{D2}{}^{\delta+}P_{D1}{}^{\delta-}Chl_{D1})^*_{673nm}$ and $(Chl_{D1}{}^{\delta+}Phe_{D1}{}^{\delta-})^*_{681nm}$ (where the subscript indicates the approximate center wavelength of the electronic transition for each mixed state). Moreover, the CT state $P_{D2}{}^{+}P_{D1}{}^{-}$ acquires excited state character due to its mixing with an exciton, producing the $(P_{D2}{}^{+}P_{D1}{}^{-})^{\delta*}_{684nm}$ CT-exciton state, which is also able to initiate charge separation.

In addition, the results show that the pigment-protein interactions fine-tune the energy of the exciton and CT states, and hence the mixing between these states, which ultimately controls the selection and efficiency of a specific charge separation pathway.

SUPPORTING MATERIAL

Two tables, five figures, and references are available at http://www.biophysj.org/biophysj/supplemental/S0006-3495(12)00683-2.

This work was supported by a Marie Curie fellowship within the Research Training Network INTRO2 (MRTN-CT-505069 to E.R.), the Netherlands Organization for Scientific Research-Chemical Sciences (TOP grant 700.58.305 to R.v.G.), and the European Research Council (Advanced Grant proposal 267333 (PHOTPROT) to R.v.G.).

REFERENCES

1. Zouni, A., H. T. Witt, …, P. Orth. 2001. Crystal structure of photosystem II from *Synechococcus elongatus* at 3.8 A resolution. *Nature.* 409:739–743.
2. Ferreira, K. N., T. M. Iverson, …, S. Iwata. 2004. Architecture of the photosynthetic oxygen-evolving center. *Science.* 303:1831–1838.
3. Loll, B., J. Kern, …, J. Biesiadka. 2005. Towards complete cofactor arrangement in the 3.0 A resolution structure of photosystem II. *Nature.* 438:1040–1044.
4. Guskov, A., J. Kern, …, W. Saenger. 2009. Cyanobacterial photosystem II at 2.9-A resolution and the role of quinones, lipids, channels and chloride. *Nat. Struct. Mol. Biol.* 16:334–342.
5. Umena, Y., K. Kawakami, …, N. Kamiya. 2011. Crystal structure of oxygen-evolving photosystem II at a resolution of 1.9 Å. *Nature.* 473:55–60.
6. Barter, L. M. C., J. R. Durrant, and D. R. Klug. 2003. A quantitative structure-function relationship for the photosystem II reaction center: supermolecular behavior in natural photosynthesis. *Proc. Natl. Acad. Sci. USA.* 100:946–951.
7. Durrant, J. R., D. R. Klug, …, J. P. Dekker. 1995. A multimer model for P680, the primary electron donor of photosystem II. *Proc. Natl. Acad. Sci. USA.* 92:4798–4802.
8. van Brederode, M. E., and R. van Grondelle. 1999. New and unexpected routes for ultrafast electron transfer in photosynthetic reaction centers. *FEBS Lett.* 455:1–7.
9. van Brederode, M. E., F. van Mourik, …, R. van Grondelle. 1999. Multiple pathways for ultrafast transduction of light energy in the photosynthetic reaction center of *Rhodobacter sphaeroides*. *Proc. Natl. Acad. Sci. USA.* 96:2054–2059.
10. Novoderezhkin, V. I., E. G. Andrizhiyevskaya, …, R. van Grondelle. 2005. Pathways and timescales of primary charge separation in the photosystem II reaction center as revealed by a simultaneous fit of time-resolved fluorescence and transient absorption. *Biophys. J.* 89:1464–1481.
11. Novoderezhkin, V. I., J. P. Dekker, and R. van Grondelle. 2007. Mixing of exciton and charge-transfer states in Photosystem II reaction centers: modeling of Stark spectra with modified Redfield theory. *Biophys. J.* 93:1293–1311.
12. Romero, E., I. H. M. van Stokkum, …, R. van Grondelle. 2010. Two different charge separation pathways in photosystem II. *Biochemistry.* 49:4300–4307.
13. Novoderezhkin, V. I., E. Romero, …, R. van Grondelle. 2011. Multiple charge separation pathways in photosystem II: modeling of transient absorption kinetics. *ChemPhysChem.* 12:681–688.
14. Boxer, S. G. 1996. Stark spectroscopy of photosynthetic systems. *In* Biophysical Techniques in Photosysnthesis. J. Amesz and A. J. Hoff, editors. Kluwer Academic Publishers, Dordrecht. 177–189.
15. Bublitz, G. U., and S. G. Boxer. 1997. Stark spectroscopy: applications in chemistry, biology, and materials science. *Annu. Rev. Phys. Chem.* 48:213–242.
16. Liptay, W. 1974. *In* Excited States, E. Lim, editor. Academic Press, New York. 129–229.
17. Frese, R. N., M. Germano, …, J. P. Dekker. 2003. Electric field effects on the chlorophylls, pheophytins, and β-carotenes in the reaction center of photosystem II. *Biochemistry.* 42:9205–9213.
18. Giorgi, L. B., P. J. Nixon, …, D. R. Klug. 1996. Comparison of primary charge separation in the photosystem II reaction center complex isolated from wild-type and D1-130 mutants of the cyanobacterium *Synechocystis* PCC 6803. *J. Biol. Chem.* 271:2093–2101.
19. Shibuya, Y., R. Takahashi, …, T. Noguchi. 2010. Hydrogen bond interactions of the pheophytin electron acceptor and its radical anion in photosystem II as revealed by Fourier transform infrared difference spectroscopy. *Biochemistry.* 49:493–501.
20. Diner, B. A., E. Schlodder, …, D. A. Chisholm. 2001. Site-directed mutations at D1-His198 and D2-His197 of photosystem II in

Synechocystis PCC 6803: sites of primary charge separation and cation and triplet stabilization. *Biochemistry.* 40:9265–9281.

21. Schlodder, E., T. Renger, …, B. A. Diner. 2008. Site-directed mutations at D1-Thr179 of photosystem II in *Synechocystis* sp. PCC 6803 modify the spectroscopic properties of the accessory chlorophyll in the D1-branch of the reaction center. *Biochemistry.* 47:3143–3154.
22. Schlodder, E., W. J. Coleman, …, B. A. Diner. 2008. Site-directed mutations at D_1-His198 and D_1-Thr179 of photosystem II in *Synechocystis* PCC 6803: deciphering the spectral properties of the PSII reaction center. *Philos. Trans. R. Soc. B. Biol. Sci.* 363:1197–1202.
23. Kwa, S. L. S., W. R. Newell, …, J. P. Dekker. 1992. The reaction center of photosystem II studied with polarized fluorescence spectroscopy. *Biochim. Biophys. Acta.* 1099:193–202.
24. Beekman, L. M. P., M. Steffen, …, R. van Grondelle. 1997. Characterization of the light-harvesting antennas of photosynthetic purple bacteria by Stark spectroscopy. 1. LH1 antenna complex and the B820 subunit from *Rhodospirillum rubrum*. *J. Phys. Chem. B.* 101:7284–7292.
25. Frese, R. N., M. A. Palacios, …, J. P. Dekker. 2002. Electric field effects on red chlorophylls, β-carotenes and P700 in cyanobacterial photosystem I complexes. *Biochim. Biophys. Acta.* 1554:180–191.
26. Lösche, M., G. Feher, and M. Y. Okamura. 1987. The Stark effect in reaction centers from *Rhodobacter sphaeroides* R-26 and *Rhodopseudomonas viridis*. *Proc. Natl. Acad. Sci. USA.* 84:7537–7541.
27. Lockhart, D. J., and S. G. Boxer. 1988. Stark effect spectroscopy of *Rhodobacter sphaeroides* and *Rhodopseudomonas viridis* reaction centers. *Proc. Natl. Acad. Sci. USA.* 85:107–111.
28. Middendorf, T. R., L. Mazzola, …, S. G. Boxer. 1993. Stark effect (electroabsorption) spectroscopy of photosynthetic reaction centers at 1.5 K: evidence that the special pair has a large excited-state polarizability. *Biochim. Biophys. Acta.* 1143:223–234.
29. Nanba, O., and K. Satoh. 1987. Isolation of a photosystem II reaction center consisting of D-1 and D-2 polypeptides and cytochrome b-559. *Proc. Natl. Acad. Sci. USA.* 84:109–112.
30. Dekker, J. P., N. R. Bowlby, and C. F. Yocum. 1989. Chlorophyll and cytochrome *b-559* content of the photochemical reaction center of photosystem II. *FEBS Lett.* 254:150–154.
31. Groot, M. L., E. J. G. Peterman, …, R. van Grondelle. 1995. Triplet and fluorescing states of the CP47 antenna complex of photosystem II studied as a function of temperature. *Biophys. J.* 68:281–290.
32. Groot, M.-L., R. N. Frese, …, J. P. Dekker. 1999. Spectroscopic properties of the CP43 core antenna protein of photosystem II. *Biophys. J.* 77:3328–3340.
33. Raszewski, G., B. A. Diner, …, T. Renger. 2008. Spectroscopic properties of reaction center pigments in photosystem II core complexes: revision of the multimer model. *Biophys. J.* 95:105–119.
34. Raszewski, G., W. Saenger, and T. Renger. 2005. Theory of optical spectra of photosystem II reaction centers: location of the triplet state and the identity of the primary electron donor. *Biophys. J.* 88:986–998.
35. Dekker, J. P., and R. Van Grondelle. 2000. Primary charge separation in photosystem II. *Photosynth. Res.* 63:195–208.
36. Peterman, E. J., H. van Amerongen, R. van Grondelle, and J. P. Dekker. 1998. The nature of the excited state of the reaction center of photosystem II of green plants: a high-resolution fluorescence spectroscopy study. *Proc. Natl. Acad. Sci. USA.* 95:6128–6133.
37. Kwa, S. L. S., C. Eijckelhoff, …, J. P. Dekker. 1994. Site-selection spectroscopy of the reaction center complex of photosystem II. 1. Triplet-minus-singlet absorption difference: search for a second exciton band of P-680. *J. Phys. Chem.* 98:7702–7711.